5

Temporal pulse tailoring in laser manufacturing technologies

Razvan Stoian[1], Matthias Wollenhaupt[2], Thomas Baumert[2], and Ingolf V. Hertel[3,4]

[1] Laboratoire Hubert Curien, UMR 5516 CNRS, Université Jean Monnet, 42000 Saint Etienne, France razvan.stoian@univ-st-etienne.fr
[2] Institut für Physik and CINSaT, Universität Kassel, 34132 Kassel, Germany wollenhaupt@physik.uni-kassel.de; baumert@physik.uni-kassel.de
[3] Max Born Institute for Nonlinear Optics and Short Pulse Spectroscopy, 12489 Berlin, Germany, hertel@mbi-berlin.de
[4] Fachbereich Physik, Freie Universität Berlin, 14195 Berlin, Germany

Abstract. Ultrafast lasers have gained momentum in material processing technologies in response to requirements for higher accuracy. Minimal energy diffusion and high nonlinearity of interaction indicate the possibility of confining energy on the smallest scales. The possibility of temporal beam manipulation allows adapting the incoming energy rate to the material individual reaction. Optimal energy coupling gives thus the possibility to guide the material response towards user-designed directions, offering extended flexibility for quality material processing.

5.1 Introduction

The demand for precision in laser material processing requires the development of irradiation tools that are able to localize the energy on small temporal and spatial scales. Ultrashort laser pulses have therefore become instruments of choice for material structuring on a micro- or even nanometer scale. The high nonlinearity of the interaction, good energy confinement, and limited heat diffusion offer challenging perspectives for judiciously designed direct structuring processes, as well as for applications in nanosurgery, generation of nanoparticles, or minimally invasive ablation for spectroscopic purposes (see e.g. Chapters 6 and 8 of this book). However, new laser machining requirements are imposing higher standards for optimal processing, envisaging possibly reconfigurable technologies that are matter- and shape-adaptable in a self-improving manner. This goal may be achieved by smart manipulations of the laser beam in the spatio-temporal domain and by complex monitoring of the ablation products for optimizing irradiation parameters. Light modulation as a function of the materials reaction implies that a synergetic type of interaction occurs between radiation and material which offers the possibility

to regulate and actively improve the energy delivery. Recent technologies allow flexible manipulation of laser pulse characteristics, including its temporal form, spatial distribution, spectral content, and polarization state. The energy delivery can be adaptively controlled to guide the material response towards a designed processing objective. Higher accuracy and novel material states may be obtained in this way that involves a radical change in the materials standard response. The tailored interaction has an engineering aspect, related to a precise definition of the excitation geometry, as well as a phenomenological one, associated with controlling laser-induced physical phenomena. With the focus on the latter, the present review summarizes several concepts of pulse manipulation, emphasizing ultrafast pulse tailoring in the temporal domain, and explore its potential in applications to material processing.

Primary processes induced by ultrafast laser radiation involve nonlinear electronic excitation, energy transfer to vibration modes, and phase transitions that occur on fast but material dependent time scales. Temporal laser control may thus facilitate synchronization between light and material response, thus leading to efficient coupling of laser energy. In addition, new insights become available concerning the physical effects of irradiation. However, due to the complexity of interaction, optimal irradiation conditions require optimal search procedures which allow to explore complicated and often only moderately sensitive parameter topologies. Parameter landscapes can be built in this way to determine relevant processing protocols and to collect information on the control mechanisms. The capacity to predict best irradiation conditions is paramount to smart laser processing technologies that can accommodate dynamic material reactions, thus responding to a maximum of user demands.

After this introduction, section 5.2 will review basic laser pulse properties together with practical concepts of pulse manipulation in the spectral Fourier domain. Specifically, the possibility to control pulse characteristics in a programmable way using present light-modulator devices will be discussed in subsection 5.2.5. Optimization strategies will be indicated in section 5.2.6. Section 5.3 will then present selected aspects of application of these techniques in material processing, starting in section 5.3.1 with a discussion of the primary physical factors prone to play a fundamental role in controlling energy coupling and the time evolution of excited matter. Electronic excitation aspects as well as the possibility to drive specific thermodynamic trajectories in metals and semiconductors upon relaxation (section 5.3.2) will be discussed. Insights will be given into the generation of electron-hole plasmas in band-gap materials or electronic heating in metals, emphasizing the consequences for the subsequent transient states of matter, including the possibility to adaptively achieve specific thermodynamic and mechanical states. Advances in surface texturing will be indicated, pointing out the potential for nanoscale processing. The presentation will follow how the dynamic light regulation creates the premises to upgrade the degree of process control. Finally, section 5.3.3 will consider practical implementation for processing bulk dielectrics.

5.2 Fundamental and technical aspects of pulse shaping

5.2.1 Basics of ultrashort laser pulses

With very few exceptions, the generation of ultrashort pulses relies on the technique of mode locking and is described in detail in several textbooks devoted to ultrashort laser pulses [1–3]. An ultrashort laser pulse can be viewed as a Fourier-synthesized object with a large spectral bandwidth containing on the order of 10^6 longitudinal laser modes. In a Fourier-transformed pulse all frequencies are locked. Manipulation of these frequencies in phase and amplitude constitutes the key tool for changing the temporal structure.

5.2.2 Frequency domain manipulation (mathematical formalism)

Assuming a linearly polarized light field, the temporal dependence of the real electric field $E(t)$ of an optical pulse may be written as a rapidly oscillating scalar quantity (with a time dependent overall phase $\Phi(t)$) which is multiplied by a real valued temporal envelope function $A(t$:

$$E\left(t\right) = A\left(t\right)\cos\left[\Phi(t)\right] = A\left(t\right)\cos\left[\zeta\left(t\right) + \omega_0 t\right] \quad .$$

Here ω_0 is the carrier frequency and $\zeta\left(t\right)$ a temporal phase. Changes of the instantaneous frequency $\omega\left(t\right)$ are described by the derivative of the temporal phase $\zeta\left(t\right)$, i.e. $\Delta\omega\left(t\right) = \frac{d}{dt}\zeta\left(t\right)$. The real-valued electric field $E(t)$ of an ultrashort optical pulse at a fixed point in space and its equivalent in frequency space $\widetilde{E}\left(\omega\right)$ (possibly complex-valued) are related by the Fourier transform which we write as [1, 3, 4]

$$\widetilde{E}(\omega) = \int_{-\infty}^{\infty} E\left(t\right)\mathrm{e}^{-\mathrm{i}\omega t}dt \quad .$$

The knowledge of the spectrum for positive frequencies is sufficient for a full characterization and in the following we consider $\widetilde{E}^{+}\left(\omega\right) = \widetilde{E}\left(\omega\right)$ for $\omega > 0$. Inverse Fourier transform of $\widetilde{E}^{+}(\omega)$ delivers the analytic signal

$$E^{+}(t) = \frac{1}{2\pi}\int_{0}^{\infty} \widetilde{E}^{+}(\omega)\,\mathrm{e}^{\mathrm{i}\omega t}d\omega \quad ,$$

which is decomposed into the pulse envelope $\mathcal{E}^{+}(t)$ and the carrier oscillation by $E^{+}(t) = \mathcal{E}^{+}(t)\,\mathrm{e}^{\mathrm{i}\omega_0 t}$. Fourier transform of the temporal envelope $\mathcal{E}^{+}(t)$ yields the spectrum of the envelope $\widetilde{\mathcal{E}}^{+}(\omega) = \widetilde{E}^{+}(\omega+\omega_0)$ and its power spectral density $I(\omega) \propto |\widetilde{\mathcal{E}}^{+}(\omega)|^2$. This is displayed along with the temporal intensity $I(t) \propto |\mathcal{E}^{+}(t)|^2$ for various modulated pulses in Figs. 5.1-5.5.

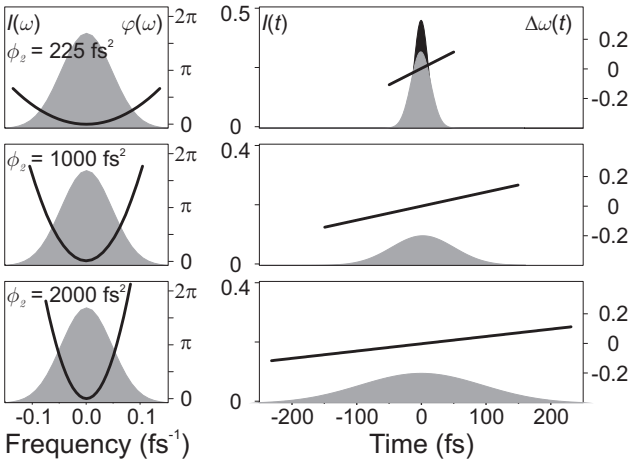

Fig. 5.1. Left: Quadratic spectral phase modulation with $\varphi(\omega) = \phi_2/2! \cdot \omega^2$ for increasing GDD ϕ_2 applied to the spectrum $I(\omega)$ of a Gaussian input pulse of $\Delta t = 25\,\mathrm{fs}$ (the carrier frequency is subtracted). Right: temporal intensity envelope $I(t)$ of the modulated pulse and change of the instantaneous frequency $\Delta\omega(t)$. The GDD increases from $225\,\mathrm{fs}^2$ to $2000\,\mathrm{fs}^2$. For comparison, the unmodulated pulse (in the background) is depicted in the upper panel

In order to describe changes in the temporal pulse shape due to spectral manipulations it is convenient to characterize the passage of an ultrashort pulse through a linear optical system by a complex optical transfer function [5]

$$\widetilde{M}(\omega) = \widetilde{R}(\omega)\,\mathrm{e}^{-\mathrm{i}\varphi(\omega)} \quad ,$$

connecting the incident electric field envelope $\widetilde{\mathcal{E}}^{+}_{in}(\omega)$ with the modulated one

$$\widetilde{\mathcal{E}}^{+}_{mod}(\omega) = \widetilde{M}(\omega)\,\widetilde{\mathcal{E}}^{+}_{in}(\omega) = \widetilde{R}(\omega)\,\mathrm{e}^{-\mathrm{i}\varphi(\omega)}\widetilde{\mathcal{E}}^{+}_{in}(\omega) \quad .$$

Here $\widetilde{R}(\omega)$ is the real valued spectral amplitude response and $\varphi(\omega)$ the so called spectral phase transfer function. This is the phase accumulated by the spectral component of the pulse at frequency ω upon propagation through the optical system. Due to the properties of the Fourier transform, the multiplication in the frequency domain corresponds to a convolution in time domain:

$$\mathcal{E}^{+}_{mod}(t) = \frac{1}{2\pi}\int_{-\infty}^{\infty}\widetilde{M}(\omega)\,\widetilde{\mathcal{E}}^{+}_{in}(\omega)\,\mathrm{e}^{\mathrm{i}\omega t}d\omega = \int_{-\infty}^{\infty}M(t-t')\,\mathcal{E}^{+}_{in}(t')\,dt' \quad .$$

In the following we will concentrate mainly on pure phase modulation and therefore set $\widetilde{R}(\omega) = 1$ for all frequencies. For quantitative comparison of experimental results obtained by temporal modulated pulses with those obtained using unmodulated pulses, pure phase modulation guarantees that the sample is exposed to the same pulse energy and the same spectrum, the only difference being the temporal distribution of the laser radiation.

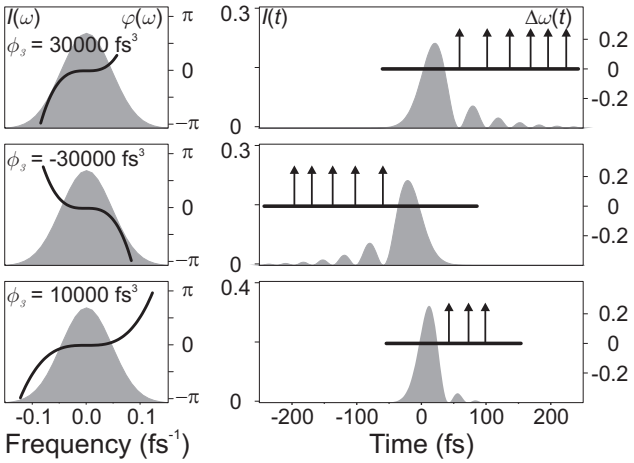

Fig. 5.2. TOD spectral phase functions $\varphi(\omega) = \phi_3/3! \cdot \omega^3$ (left) and temporal intensities (right) for positive and negative ϕ_3. The arrows indicate a change of sign in the temporal envelope, corresponding to a jump of the temporal phase by π

5.2.3 Analytical phase functions relevant to material processing

Polynomial phase functions

A simple approach to understand the physical significance of a spectral phase function $\varphi(\omega)$ with respect to the temporal pulse shape is based on its Taylor expansion resulting in a sum of polynomial phase functions:

$$\varphi(\omega) = \phi_0 + \phi_1\omega + \frac{\phi_2}{2!}\omega^2 + \frac{\phi_3}{3!}\omega^3 + \ldots \quad . \tag{5.1}$$

The absolute phase, which relates the carrier oscillation to the envelope, is modulated if the first term ϕ_0 is non-zero. Although this type of modulation can be important for coherent control experiments [6], it does not influence the pulse envelope and is therefore not considered here. In accordance with the Fourier shift theorem, the linear term in the spectral modulation function $\phi_1\omega$ is responsible for a time shift of the pulse envelope of $t = \phi_1$.

Quadratic phase modulation, the so called Group Delay Dispersion GDD= ϕ_2 with a spectral phase function $\varphi(\omega) = \phi_2/2! \cdot \omega^2$ plays a major role in many applications (see e.g. [7] and ref. there). GDD modifies the laser pulse duration and introduces a linear frequency sweep. Fig. 5.1 shows the influence of GDD on a Gaussian input pulse. With increasing chirp parameter ϕ_2 the pulse duration increases while the pulse intensity decreases correspondingly.

Third Order Dispersion TOD=ϕ_3 is given by a spectral phase function $\varphi(\omega) = \phi_3/3! \cdot \omega^3$ and results in asymmetric pulses described by a damped Airy function [3, 8]. Fig. 5.2 shows examples for TOD spectral phase modulation for positive and negative values of the parameter ϕ_3, as well as a variation of

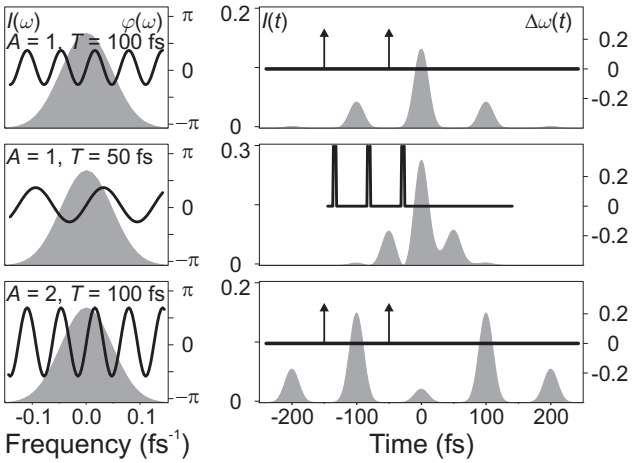

Fig. 5.3. Upper panel: sinusoidal spectral phase modulation with $A = 1$; $T = 100\,\mathrm{fs}$, $\phi = 0$. Middle: lowering the modulation frequency to $T = 50\,\mathrm{fs}$ merges the sub-pulses. Increasing the amplitude A results in a higher number of sub-pulses. The arrows indicate again a phase change by π

the absolute value of ϕ_3. The pulse shape is characterized by an intense initial pulse followed or preceded by a pulse sequence with decaying amplitudes. At the zeros of the damped Airy function the temporal phase jumps by π lead to the (immaterial) delta discontinuities in the instantaneous frequency. Applying the anti-symmetric phase function of TOD results in a constant instantaneous frequency. With respect to material processing the remarkable features of TOD are (*i*) temporal symmetry-breaking of the envelope implying control on the time-dependent energy flux onto the sample and (*ii*) the ability to produce a short intense pulse accompanied by a weak long pulse train.

Pulse sequences

Pulse sequences are a common tool to study dynamical properties of light matter interactions and have also found applications to ultrafast material processing [9]. Using an interferometric setup is conceptually the simplest way to produce a sequence of pulses. However, practical considerations, such as the stability and alignment issues, but most importantly the unavoidable spectral modulations introduced by the interferometer, suggest alternative approaches based on pulse shaping techniques. We discuss here three different types of phase functions leading to pulse sequences [10].

Periodic spectral phase functions applied to modulate the spectrum of an ultrafast laser pulse deliver pulse sequences of controllable intensity, phase and temporal separation. It has been shown [3,10–15] that a sinusoidal spectral phase modulation $\varphi(\omega) = A\sin(\omega T + \phi)$ leads to a sequence of sub-pulses with a temporal separation T and controllable relative temporal phases

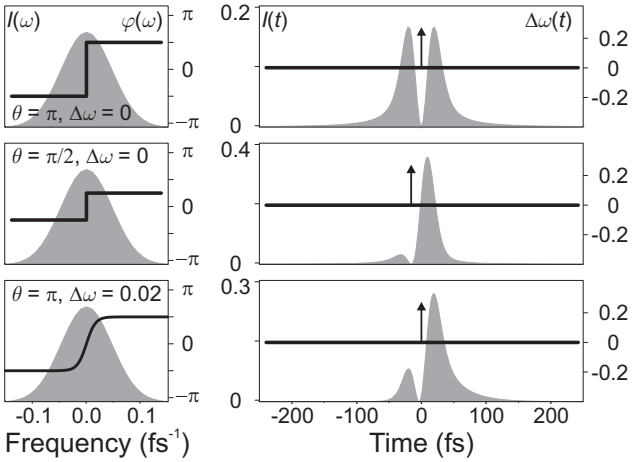

Fig. 5.4. Spectral phase function with a θ-step at the central frequency. Upper panel: $\theta = \pi$ leads to symmetric picosecond double pulses, middle: $\theta = \pi/2$ results in a weak pre-pulse and an intense post-pulse, lower trace: blurring the π-step reduces the pulse duration

determined by the absolute phase ϕ:

$$\mathcal{E}^{+}_{mod}(t) = \sum_{n=-\infty}^{\infty} J_n(A)\, \mathcal{E}^{+}_{in}(t - nT)\, e^{-in\phi} \quad .$$

The amplitude of the n-th sub-pulse is given by Bessel functions $J_n(A)$ of the first kind and order n and can be controlled by the modulation parameter A. Provided the individual sub-pulses are temporally separated, the envelope of each sub-pulse is a replica of the unmodulated pulse envelope (Fig. 5.3 upper and lower panel). The arrows between the sub-pulses indicate a change-of-sign in the pulse envelope. For smaller delay times T the sub-pulses interfere to yield a more structured pulse shape (Fig. 5.3 middle panel).

Spectral phase jumps based on discontinuous functions of the type $\theta\,\mathrm{sgn}/2$ were realized [10] to produce a sequence of two pulses. Such pulses have e.g. been used to manipulate coherent atomic dynamics [6,16,17]. An example for a discontinuity of π at the central frequency in the spectral phase function is shown in the upper panel of Fig. 5.4. This so-called π-step results in two pulses with larger duration and delayed with respect to each other. A slight generalization of this spectral phase is introduced by variation of the step-height. A phase jump of $\pi/2$ breaks the temporal symmetry and is associated with a weak pre-pulse and an intense post-pulse (middle panel of Fig. 5.4). Due to this structure, generalized jumps might be suitable candidates for materials processing similar to TOD. Blurring the phase discontinuity is an alternative approach to deliver asymmetric pulses. In addition, blurred phase functions deliver much shorter pulses (reduced tails) – a property which is required to

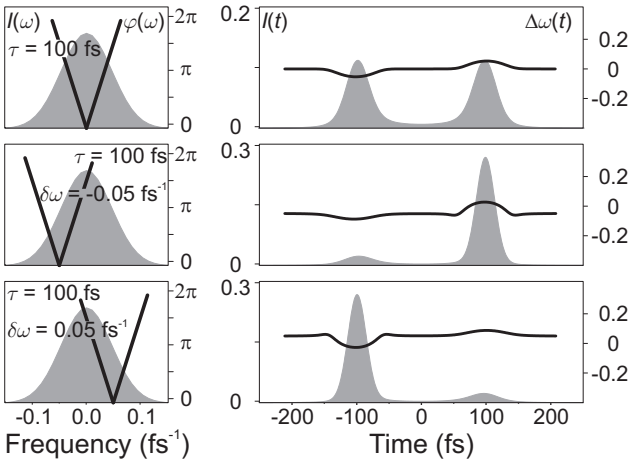

Fig. 5.5. An upright V-shaped spectral phase $\varphi(\omega) = \tau|\omega - \delta\omega|$ creates a sequence of a red-detuned pre-pulse and a blue-detuned post-pulse: each portion of the spectrum where the phase is linear corresponds to a longer pulse shifted by $\pm\tau$

manipulate ultrafast dynamics on the sub-picosecond level. Cycling the phase jump can also generate multiple pulses of variable spacing [18], however with considerable spatio-temporal distortions [19, 20].

V-shaped function impose linear phase relations on chosen spectral domains [21]. The phase function $\varphi(\omega) = \tau|\omega - \delta\omega|$ shown in Fig. 5.5 can generate a sequence of two pulses separated by 2τ. This type of modulation can be understood in terms of the shifting property of linear phase functions. In the upper panel of Fig. 5.5 half the spectrum is shifted by $t = -\tau$ whereas the other half of the spectrum is moved to $t = +\tau$. This procedure results in two detuned coloured pulses with longer durations. The relative intensity ratio is determined by the cusp position. By mirroring the spectral phase function with respect to the central frequency, the temporal envelope is reversed and the temporal phase is conjugated.

Linear combinations of the above phase masks

If a sum of multiple spectral phase functions $\varphi_i(\omega)$ is applied, the combined action of the linear combination can be decomposed into subsequent execution of the corresponding individual phase functions:

$$\widetilde{M}(\omega) = \mathrm{e}^{-\mathrm{i}[\varphi_1(\omega)+\varphi_2(\omega)]} = \mathrm{e}^{-\mathrm{i}\varphi_1(\omega)}\mathrm{e}^{-\mathrm{i}\varphi 2(\omega)} = \widetilde{M}_1(\omega)\,\widetilde{M}_2(\omega)$$

For example, combining sinusoidal phase modulation with quadratic phase function yields a sequence of chirped pulses [22]. Double pulses can also be implemented with the help of amplitude modulation [23, 24]. The spectral transfer function reduces to a real valued spectral amplitude response [23].

In general, the outcome of combinations of spectral phase functions on the temporal pulse shape is not always easy to predict due to interference effects among the subsequent modulations.

Iterative Fourier approaches for designing pulse shapes

In the situation that required pulse shapes are not readily accessible by the above methods, an accurate solution can only be based on a combined phase and amplitude modulation procedure. However, if a phase-only solution is preferred, techniques have emerged were approximate solutions to the desired shape, which are based on phase modulation, are found using iterative transformations between the temporal and the spectral domains in the presence of constraints related to the incident pulse spectrum and the desired shape. An intuitive description of the Gerchberg-Saxton technique is given in [25, 26].

Polarization shaped pulses in the temporal domain

Since light is a transverse electromagnetic wave, it can be linearly, circularly or in general elliptically polarized. The same holds of course for an ultrashort optical pulse. Pulse shaping allows for the creation of light pulses where at each instant of time a different state of polarization can be realized [27, 28]. So far these possibilities have not been exploited in material processing, but might open up interesting perspectives for future use. Specifically, this may involve controlling nanoscale phenomena, near-field and plasmon coupling, with extended possibilities for novel processing techniques.

5.2.4 Pulse shaping in the spatial domain

Tailoring of spatial intensities has also acquired a significant attention and implications are obvious in material processing, microscopy, imaging, and nonlinear optics. The application field will only be briefly reminded, with implications in control of wavefront distortions and corrective approaches for beam delivery, point-spread-function engineering and design of excitation geometries, as well as concepts for beam partition for parallel processing.

5.2.5 Experimental implementations for temporal pulse shaping

In practice, the creation of complex shaped laser pulses with respect to phase, amplitude and polarization relies on programmable pulse shaping techniques [3, 5, 18] to generate the optical transfer function $\widetilde{M}(\omega)$. One way to realize a pulse modulation unit is the Fourier transform pulse shaper. Its operation principle is based on optical Fourier transformation between time and frequency domains. In Fig. 5.6a a standard design of such a Fourier synthesis pulse shaper is sketched. The incoming ultrashort laser pulse is spectrally

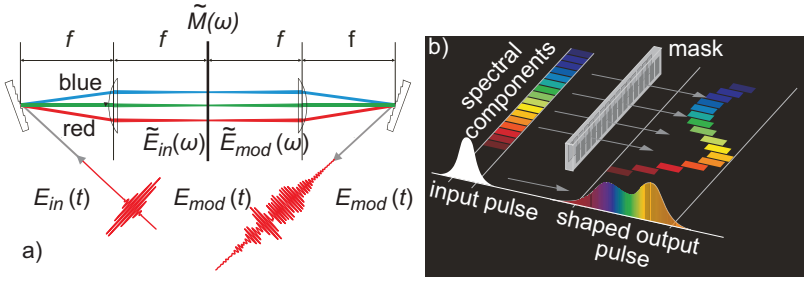

Fig. 5.6. (a) Basic layout for Fourier transform femtosecond pulse shaping. (b) Schematic illustration of shaping the temporal profile of an ultrashort laser pulse by retardation of the spectrally dispersed individual wavelength components in a phase only LC-SLM. The LC-SLM is located in the Fourier plane

dispersed and the frequency components are back collimated by a focusing optical element with a focal distance f. By this means, the spectral components can be modulated individually by placing a linear mask into the Fourier plane. The laser pulse is reconstructed by performing an inverse Fourier transformation back into the time domain [29].

A popular linear mask for computer controlled pulse shaping in such setups is the Liquid Crystal Spatial Light Modulator (LC-SLM). The relative retardation of spatially dispersed frequencies can be conveniently manipulated by placing a pixelated liquid-crystal array in the Fourier plane and applying voltages at the separate pixels leading to changes of the refractive index. By virtue of the Fourier transform properties, spectral phase changes result in modulated pulse temporal profiles as depicted schematically in Fig. 5.6b. Exploiting the LC orientation with respect to the polarization, amplitude modulation may be obtained as well based on the induced birefringence [18, 30].

Another possibility to realize phase only pulse shaping is based on deformable mirrors (DM) [31] placed in the Fourier plane. They usually consist of a small number of control degrees of freedom. The use of a micro mirror array with 240×200 pixels in reflection and a waveform update rate larger than 1 kHz was also demonstrated [32].

Acousto optic modulators (AOMs) can be used for programmable pulse shaping within $4f$ setups in various spectral domains [33–35]. The AOM crystal oriented at Bragg angle is placed in the Fourier plane of a zero dispersion compressor. A programmable radio frequency (RF) signal driving the piezoelectric transducer of the AOM creates an acoustic wave that propagates through the crystal. The photoelastic effect induces a modulated grating where the amplitude and phase of the acoustic wave determine the diffraction efficiency and phase shift at each point in space.

Another AOM approach is based on an acousto-optic programmable dispersive filter (AOPDF) which does not need insertion in the Fourier plane of a $4f$ device [36, 37] but relies instead on the time convolution. Again, a pro-

grammable RF signal creates an acoustic wave that propagates in the crystal and reproduces spatially the temporal shape of the RF signal. Two optical modes can be coupled by acousto-optic interaction only in the case of phase matching. If there is locally a unique spatial frequency in the acoustic grating, then only one optical frequency can be diffracted at that position from the fast ordinary axis to the slow extraordinary axis. Various groups of optical frequency components travel a different distance before they encounter phase matched spatial frequencies in the acoustic grating where the energy is diffracted from one axis to the other. The modulated pulse will be made of all spectral components that have been diffracted at the various positions, with amplitudes controlled by the acoustic power and retardation given by the velocity difference.

In general pulse shapers based on LC-SLMs or on DMs have low transmission losses, do not impose additional chirp and have a low waveform update rate on the order of 10 Hz. Setups based on AOMs have high transmission losses, they do impose additional chirp but they have a waveform update rate in the order of 100 kHz. Both AOMs and LC-SLMs can impress in the order of 1000 independent features onto the spectrum and are suitable for amplitude and phase modulation. Programmable polarization shaping has been demonstrated so far only with LC-SLMs.

The pulse shaping techniques described up to now allow control of the temporal profile of an output waveform in phase, amplitude, and polarization. This can be thought of as control over one spatial dimension, the direction of propagation, and the "temporal-only" pulse shaping is thus one dimensional. Automated two dimensional phase-only pulse shaping employing an optically addressed reflective two-dimensional SLM with negligible interpixel gaps allows real-space pulse shaping in which a sample or device is irradiated with different temporally shaped waveforms at different locations [38]. The pulse shaping arrangement in [38] is similar to conventional $4f$ spectral filtering arrangements, with the difference that the incoming beam is expanded in one dimension and the SLM is employed in reflection geometry.

5.2.6 Optimization strategies

Combining pulse shaping techniques with feedback learning loops (closed-loop approach) to optimize light-induced processes, a new class of experiments emerged [39–42]. As indicated in Fig. 5.7, the pulse control unit is connected to an experimental device quantifying the laser action. Then a given pulse shape is evaluated in order to produce an improved pulse form which enhances the feedback signal. The experimental output requires real-time monitoring techniques for in-situ process control. The loops are usually driven by deterministic or non-deterministic optimization algorithms, or specific pulse shapes are designed using intuitive phase masks or predictive phase-retrieval approaches (e.g. Gerchberg-Saxton). These techniques have an impact on an

increasing number of developments in physics, chemistry, biology, and engineering due to the fact that primary light-induced processes can be studied and actively controlled via adaptive femtosecond pulse shaping.

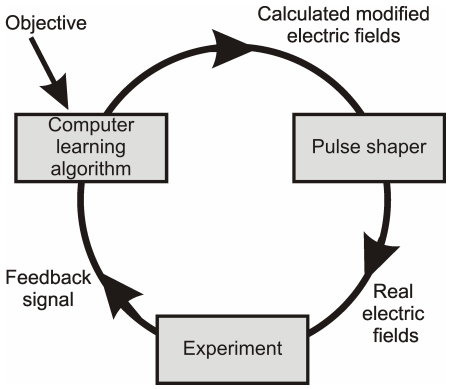

Fig. 5.7. Schematic presentation of adaptive femtosecond pulse shaping: Generated specific electric fields via a pulse shaper are tested in an experiment. A learning algorithm calculates modified electric fields based on the information from the experimental feedback signal and the user defined control objective. Cycling the loop results in iteratively optimized laser pulse shapes that finally approach the objective(s)

Often evolutionary algorithms [43] are applied, ranging from simple implementations used for example in initial automated pulse compression experiments [40] to sophisticated Covariance Matrix adaption techniques [44]. Usually, a set of arbitrary phase patterns is initially applied on the optical modulator which evolves through genetic propagators towards an optimal solution. In Ref. [44] a theoretical survey of modern evolutionary approaches to the problem of molecular alignment has been performed, concluding that it pays off to use more elaborate optimization schemes for such a high-dimensional optimization problem. It was also demonstrated that a covariance matrix adaptation evolutionary strategy (CMA-ES) performs better than a traditional evolutionary strategy for high-dimensional search landscapes [45].

If the optimization of a light-induced process is based on some physical insight, then it is often useful to use analytical phase functions (see subsec. 5.2.2) and optimize the parameters, either systematically or via evolutionary approaches. Open loops may be followed by *post mortem* analysis. An intuitive solution landscape may be built, allowing to extract useful physical information about the processes in question.

5.3 Material interaction with temporally shaped pulses

Upon impact of an ultrashort laser pulse on a solid material [46, 47], electromagnetic energy is first converted into electronic excitation and then, by specific electron-lattice interactions, transformed into thermal, chemical, and mechanical forms. During the whole process, the molecular structure and the macroscopic properties of the material are changed in various ways, culminating with permanent alterations, optical damage, and ablation. All these

processes occur on various timescales accompanied by variations of the optical properties. This suggests that the light packets interacting with the material on these timescales may accommodate the changes and create specific synergies between light and material. Optimality is then defined as the ability to achieve a user defined evolution. This section will review possible control mechanisms of laser-induced excitation and discuss their relevant timescales.

5.3.1 Control of laser-induced primary excitation events

Laser interaction with wide band-gap materials leads to the development of an electron-hole plasma. Depending on intensity, multiphoton processes (MPI) or tunneling ionization (TI) [48] are followed by inverse bremsstrahlung and subsequently by seeded collisional carrier multiplication (or avalanche ionization AI) [49–51]. The transient free carrier density plays a fundamental role in determining the optical properties, in addition to various propagation and relaxation mechanisms. Optical damage thresholds were used as experimental evidence for exceeding a certain critical electron density after the laser interaction and the regulatory effect of pulse duration was investigated [49, 52, 53]. Studies of transient electron densities range from intensities below [54, 55] up to well above the breakdown threshold [56, 57]. The temporal evolution of the free-electron population and the role of the fundamental ionization processes are strongly depending on timely energy feedthrough, as well as on the instantaneous frequency [50, 58, 59].

The excitation acquired in the two sequential steps, photoionization and free carrier absorption, offers the possibility of regulating the amount of energy coupled to the material and the outcome in terms of possible transformation paths. The absorption efficiency is controlled via the photoionization cross-section and by the timescale of electronic collisions, thus a competition between direct and collisional processes becomes possible. Each of these factors may be tuned via peak intensity, polarization state, and temporal envelope of the pulse. The direct photoionization rate in both MPI and TI regimes is mainly determined by the pulse intensity and depends on the direction of the electric field [55]. For longer temporal envelopes, a highly efficient free electron heating process develops, resulting in enhanced rates of electronic multiplication. Additionally, the electronic density may suffer fast relaxation phenomena due to, for example, carrier trapping in self-induced deformation potentials [54]. The resulting electronic density has consequences on the onset of catastrophic optical damage in band-gap dielectrics or on the structural mechanical stability. This suggests that the pulse temporal form can develop into a dominant control knob to manipulate primary excitation events and to channel possible relaxation paths in wide band-gap materials.

A situation where reduced exfoliation is displayed by structures induced in CaF_2 irradiated by modulated pulses [60] is presented in Fig. 5.8. The improvements can be related to a transient change in the material properties

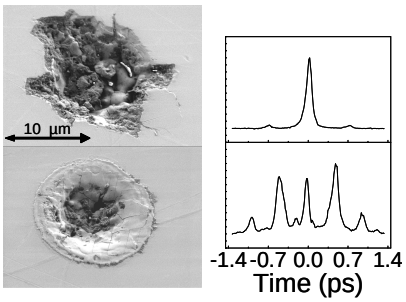

Fig. 5.8. Laser-induced structures on CaF_2 surfaces with single ultrashort pulse of 90 fs (upper part) and triple-pulse sequences (bottom part) with 0.5 ps separation. The results show improvements for the structures generated by temporally modulated excitation. The number of pulses used to form the structures was $N = 5$ and the laser fluence was $7\,\mathrm{J/cm^2}$, respectively $12\,\mathrm{J/cm^2}$ [60]

as a consequence of swift excitation and charge trapping. The sequential energy delivery induces a preparation of the surface (i.e. defined electron density and lattice deformations) and an associated material softening during the initial steps of excitation, thus changing the energy coupling for the subsequent steps. This leads to lower stress and improved structures. Especially for brittle material with strong electron-phonon coupling, carrier trapping, lattice deformations, and associated softening can be advantageous since they provide the means for relaxation of the induced stress, with a reduction of cracking and fracture phenomena. Similar behavior was also noticed during burst micromachining using multipeak sequences on MHz scales [61].

At the same time, manipulation of pulse frequencies indicated sensible variations in the damage threshold [59]. Multiple pulse sequences were used to influence the occurrence of optical damage, the profile, and the size of the induced structures in various dielectrics (a-SiO_2, Al_2O_3) [9,60,62], leading to changes in the ablation morphology. For fused silica, the temporal control on the spatial crater profile is facilitated by the synchronization with the electron trapping dynamics. The spatio-temporal coupling provided by the material nonlinearities opens the possibility to design spatial excitation features which map in space the temporal modulation of the laser pulse.

Cubic chirped pulses (with asymmetric intensity envelopes) have shown surprising reduction in the damaged area, below the diffraction limit [63,64]. The balance between photoionization and collisional ionization mediates the localized formation of a hot electron population, taking into account the different process dependencies on intensity. This results in different thresholds for material modification in fused silica and reproducible nanoscale surface structures as documented in Fig. 5.9a. As theoretical simulations based on a multiple rate equation (MRE) model [58] show, the timing of an intense photoionizing sub-pulse can turn on or off AI as illustrated in Fig. 5.9b. Different final electron densities can be achieved depending on the temporal profile since the ionization processes may be addressed in a different fashion. The proposed scenario [63] involves the interplay of MPI creating free electrons in a spatially confined region followed by AI that further restricts the area of reaching the critical electron density that may eventually lead to the nanoscale structures seen for positive and negative TOD pulses with characteristic sizes well below

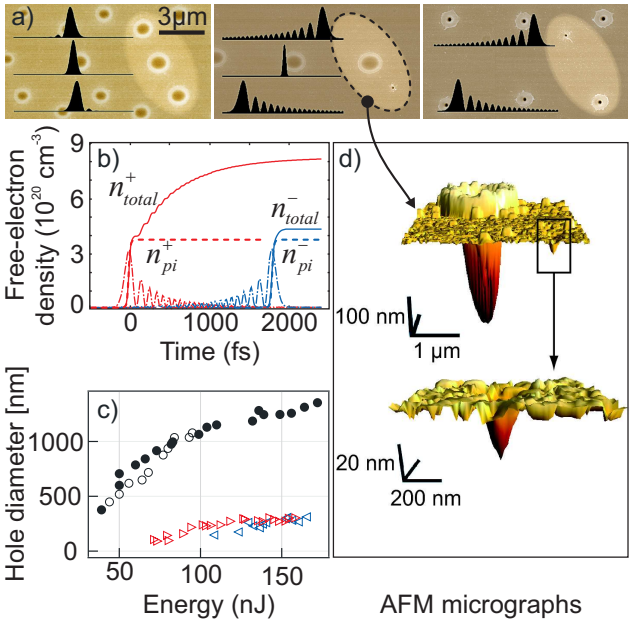

Fig. 5.9. (a) SEM images of laser-induced structures in fused silica. For a specific energy and focusing conditions (NA = 0.5, 35 fs) a triplet of applied laser pulses (negative, zero and positive TOD) is highlighted by the ellipse. Normalized temporal intensity profiles are sketched for comparison between different TODs. Left: low TOD results in negligible differences between created structures. Middle: high positive TOD results in a change of structure size and threshold energy. Right: the threshold energy for ablation with high negative TOD is reached at $E = 110$ nJ. (b) Transient free-electron density $n^{\pm}_{total}$ (solid lines) as calculated with help of the MRE, together with the density of electrons provided by photoionization $n^{\pm}_{pi}$ (dashed lines) and the corresponding transient intensities (dashed-dotted lines) of the pulse with positive TOD (index +) and negative TOD (index -), respectively. (c) Diameters of ablation structures as a function of pulse energy for unshaped pulses (different circles indicate two independent measurements), for (+) shaped pulses (triangles pointing right) and for (-) shaped pulses (triangles pointing left). Structures below 300 nm are obtained over a considerable energy range thus providing a large process window for creation of nanostructures. The smallest structures are about 100 nm in diameter.(d) Blow-up of laser-induced structures; atomic force microscope micrographs

the diffraction limit (Fig. 5.9c). This strategy opens the route to develop tailored pulse shapes for controlled nanoscale material processing of dielectrics. Note that smaller structures have been reported at the backside surface of dielectric samples by using high numerical aperture immersion objectives [65].

In metals as well, the efficiency of laser absorption depends on the electronic collision frequency, which, in the solid phase, is a sensitive function of temperature [66]. The dynamics of the electron temperature may thus influence the rate at which laser photons are absorbed. Apart from the regulating

factor of electronic collisions via temperature at nonequilibrium electron-ion conditions, the resulting transient optical properties, heat transport, and energy conversion factors may also intervene. The subsequent thermodynamic behaviour can be mastered using controlled energy feedthrough, which is a prerequisite for tailoring the laser ablation outcome, structure, and plume kinetics. An overview of possible control paths for non-transparent materials is given in the following section.

5.3.2 Engineered thermodynamic phase-space trajectories

Subsequent to primary excitation, the electronic energy is relaxed to the material matrix via electronic to vibrational coupling which locally heats the material, via bond softening caused by electronic perturbations, or is released by a pressure-induced mechanical activity. The possibility to temporally design pulses enhances the flexibility to manipulate transformation pathways using nonlinear and non-thermally initiated phase transitions, and minimally-diffusive energy input. A high degree of electronic excitation in solid materials triggers lattice instabilities and, consequently, mixed electronic, mechanical and thermal alterations of the material structure. These structural transformations occur on fast scales and a certain control on their competition may be established. This may potentially lead to the creation of metastable states around critical points or transitions to energy states hardly attainable by other means. These effects are important for surface treatment and patterning or in applications related to optical switching [67].

For semiconductor samples improvements were seen in the structuring quality by using multipulse sequences [68–70]. Synchronizing the laser temporal irradiation profile with the solid-to-liquid phase transition time and the associated augmentation in the absorption efficiency, conditions can be found to evaporate the resultant liquid layer, avoiding its gradual cooling and return to the surface as recast. Additionally, the energy delivery can control the resulting self-organization of nanotexturing in the irradiated zone [71].

Enhancement and kinetic tunability of ions was observed during temporally tailored laser irradiation of silicon. The approach has illustrated a versatile possibility to optimize the kinetic properties of the Si^+ ions by controlling the development of the electron-hole plasma on sub-ps scales [72] or by taking advantage of a fast succession of structural transitions on ps scales [73]. The latter results is shown in Fig. 5.10. The optimal irradiation sequence was obtained using a mass-resolved ion-detection optimization loop guided by an adaptive strategy and is represented by a fast peak followed by a ps tail of energy distribution. The ion acceleration mechanism was connected to an improved energy coupling related to the formation of a highly absorptive transient liquid state right at the beginning of the irradiations sequence. Most of the energy is then coupled to the absorptive state and determines significant temperatures. Highly energetic and volatile thermodynamic states are thus produced with minimal energy expenses [73].

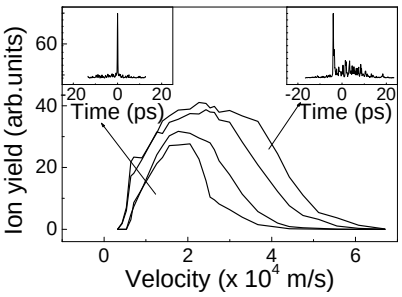

Fig. 5.10. Energetically tunable Si^+ ion beams generated by laser ablation of silicon with ultrashort and adaptively generated optimal temporal pulse shapes. Irradiation conditions: initial pulse duration 170 fs, input fluence 0.8 J/cm^2 [73]

If for the low band-gap material presented above the main factor of improving energy deposition is related to a fast change to an absorptive state, other materials show no significant differences in the dielectric function between the solid and the liquid phase at the photon energy of 1.5 eV and, therefore, no absorption enhancement. This is the case of metallic aluminum. The relevant question is then related to the factors that may improve the energy coupling in this case. Commonly for metals, electronic excitation determines a high temperature and pressure phase so that the evolution control factors involve hydrodynamic advance. This has consequences on the transient optical properties, and, equally important, on the heat transport characteristics. Feedback-based ion emission was used as a probe of the efficiency of energy deposition into the material. An ion acceleration effect was observed, similar to the Si case, and explained by a laser pulse regulated balance between the mechanical and thermal energy of the ablation products. If ultrafast radiation favours the accumulation of mechanical energy due to fast pressure release [74], the optimal picosecond tailored envelope determines a preferential heating of the ablation products which induces variations in the ionization degree, while still keeping the losses by heat conduction at a minimal level. This indicates to possibility of regulating thermal effects and designing thermodynamic trajectories and has consequences for the processing accuracy and composition of ablation products, or for other quality criteria such ablation efficiency, smoothness, or aspect ratios. On the other hand, it constitutes a description of thermal manipulation for interactions commonly considered as athermal. It has to be noted that phonon control via pulse shaping has gathered attention for regulating heat transport in laser irradiated materials [75].

In parallel to ion acceleration, a strong decrease in nanoparticle emission was observed from metallic targets irradiated with temporally shaped laser radiation. The effect, simulated by hydrodynamic codes, is illustrated in Fig. 5.11 for Al exposed to ultrashort and the previously determined optimal pulse. Ultrafast irradiation is associated with an initial isochoric increase of pressure due to electronic excitation. The pressure release determines a fast expansion into the two-phase region and ejection of nanodroplets from the liquid phase as visible in Fig. 5.11a. This is related to the trapping of expanding layers at the

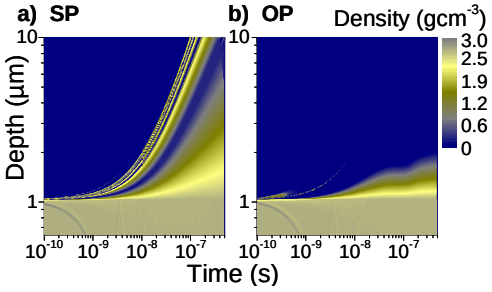

Fig. 5.11. Transient density phases and material ejection under laser excitation for (a) short and (b) optimal pulses. The onset of liquid nanolayers is observable for ultrashort pulses. The liquid layers expand under confinement between gas layers. Optimal pulses generate a preferential transition to the gas phase [76]

liquid-gas border undergoing further expansion under gas confinement, alongside with a recondensation mechanism. The tailored pulse favours instead the heating of the expanding material, reducing the trapping time of the confined liquid layers and determines a dominant transition to a gaseous phase with low particulate content [74,76]. This aspect has consequences for the rate and the dimensions of the produced nanoparticles. The validity of the adapted approach was extended for other materials for generating nanoparticles of controllable sizes [71]. The sequential energy transformation into mechanical and thermal forms creates the premises of particular phase transformations. Despite the reduced sensitivity for intensity effects in linear materials, the overall absorption efficiency can be elevated if the proper conditions for density and temperature are met for the expanding layers, with consequences for the ablation yield. Changing the composition of ablation products is a prime objective in the field of ultrafast laser-induced breakdown spectroscopy, that combines spatial resolution with spectrochemical sensitivity [77] as well as in techniques of material transfer [78].

5.3.3 Refractive index engineering by temporally tailored pulses

In that concerns bulk transparent materials, the ability to locally design the dielectric function is based on the potential balance of electronic and structural transformations associated with the refractive index change (see e.g. [79]). Chapter 9 reviews the interplay of several modification factors, including generation of defects, altering the local structure, or accumulating stress. Their relative importance can assist in engineering particular index changes in the conditions where the transformation sequence is jointly determined by the material response and the spatio-temporal character of excitation [80].

Current photoinscription techniques (for a brief review see [47, 79, 81–85] and the references therein) aim at producing positive refractive index in optical glasses, e.g. for waveguiding applications. However, the material response to optical excitation is determined by the relaxation properties of the glass. The irradiation outcome determines a complex dielectric design and electronic and structural alterations associated with either increasing or decreasing the refractive index under light exposure. In many glassy materials the standard

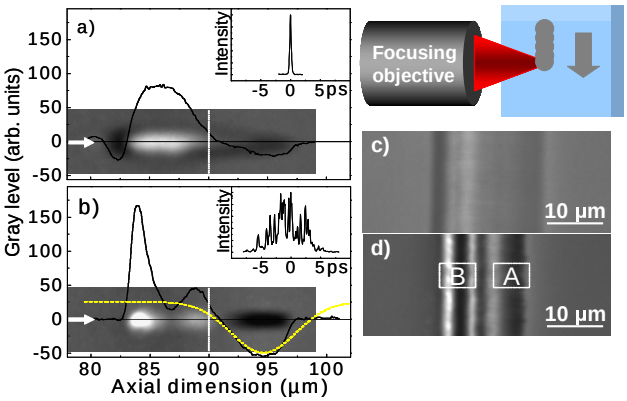

Fig. 5.12. Refractive index flip in borosilicate crown BK7 under multipulse (a) short (150 fs) and (b) optimally tailored irradiation (4.5 ps). Pulse energy 0.17 μJ, irradiation dose 10^5 pulses at 100 kHz. Phase contrast microscopy images of refractive index changes (white and black colours represent negative and positive refractive index changes, respectively). The onset of a significant compression zone is visible under optimal conditions. Transverse trace written by (c) short pulses and (d) optimal laser pulses at a scan velocity of 50 μm/s and pulse energy of 1.1 μJ. Two regions of positive refractive index changes are indicated by the labels A and B.

ultrafast radiation induces merely a decrease of the refractive index, detrimental for waveguiding. Speculatively, this is related to a strong volumetric expansion and subsequent rarefaction. Guiding regions may be restricted to stressed region around the excitation area. The possibility to reverse the natural tendency to rarefaction towards compaction carries then fundamental and technological significance. The follow-up idea is to design a type of irradiation able to overturn the unsatisfactory standard material response, with the purpose of e.g. producing positive refractive index changes in materials were the regular response is rarefaction. The temporal beam modulation techniques and subsequent control on energy delivery are natural candidates for this task due to their influence on the physical behaviour of the interaction process.

The temporal shaping approach integrated in a phase-contrast microscopy loop indicated the possibility to flip the refractive index in borosilicate crown BK7 [86] from the standard negative change to an significant region of index increase (Fig. 5.12a,b). This particular glass used here as a model material with high expansion coefficient and low softening point, usually shows a decrease of the refractive index under standard tightly-focused ultrafast laser excitation. This behaviour is associated with the formation of a hot region, where, due to rapid thermal expansion, the material is quenched in a low-density phase, rich in oxygen centres. The control mechanism is related to the design of the resultant heat source which influence the subsequent stress-induced plasticity driving axial compaction. The ps sequence allows higher energy concentration and the achievement of an elevated temperature due to

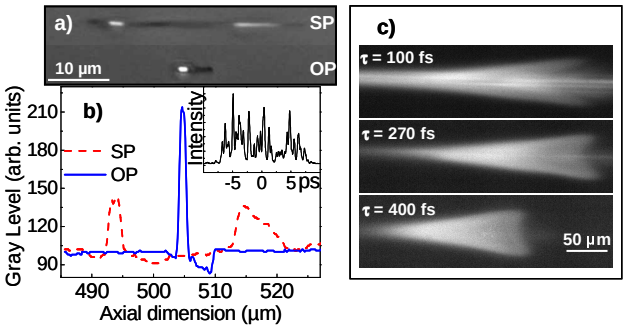

Fig. 5.13. (a) Short pulse (SP) and optimal pulse (OP) induced structures at a depth of 500 μm and 1 μJ input energy indicating the spatial confinement of the OP structure in the presence of aberrations. (b) The corresponding axial cross-sections. The inset shows the optimal pulse shape [86]. (c) Control of spatial distribution of excitation using the pulse duration [87]. Plasma emission images recorded in waveguide writing conditions in phosphate glass using different laser pulse durations and a slit shaping technique. Beam filamentation and prefocal energy depletion are minimized for circular polarization and increasing pulse durations

a less efficient plasma generation and light defocusing. This leads to plastic deformation accompanied by partial healing of the lateral stress due to preferential heat flow. As a result, a transition from a radial expansion regime to directional compaction was observed. The matter momentum relaxation leads to axial densification and to a positive refractive index change. The adaptive technique was then able to determine an excitation sequence which induces a thermo-mechanical path leading to compaction. This is particularly interesting for laser repetition rates on the timescale of mechanical relaxation (hundred kHz) and shows the importance of the heating and relaxation rates for defining proper processing windows. The influence one can exercise on the refractive index distributions indicates the possibility to create waveguide structures (Fig. 5.12c) (and symmetric guiding conditions) in materials that do not easily allow it in standard ultrafast irradiation conditions.

Adaptive control of pulse temporal forms was recently used to regulate filamentary propagation in nonlinear environments [88, 89]. The location and the spectral properties of the ionization region were shown to be modulative. The key factor is the intensity feedthrough which determines the competition between self-focusing and ionization and breakdown probability was observed to be controllable via temporal envelopes [90]. All these observations indicate flexibility in manipulating propagation, ionization, and energy gain events generated by ultrashort laser pulses in nonlinear environments using judicious intensity adjustments. The nonlinear control has consequently proven its capability to induce energy confinement even in the presence of wavefront distortions [91]. When aberrations occur, the length of the laser-induced structure augments, which is detrimental to the photoinscription precision.

The focal elongation influences the nonlinear energy deposition and modulation of the refractive index appears in the exposed region. If usually spatial corrections are applied to correct wavefront distortions, it was indicated that the energy can as well be confined using adaptive temporal pulse shaping, delivering in addition desired changes of the refractive index (Fig. 5.13a,b). The decreased nonlinearity and the lower ionization efficiency of the optimal pulse assist the energy confinement, regulating the structuring precision in the presence of wavefront distortions [91]. Furthermore, control of pulse duration was recently implemented [87] in photoinscription techniques complementary to spatial beam modulation [82,83,85,87,92] resulting in a uniform irradiation region (Fig. 5.13c) suitable for waveguide writing in phosphate glasses.

5.4 Conclusion and perspectives

The present review has illustrated that control of laser-induced effects in processing materials is possible and energy coupling can be optimized. The outcome is an improved laser structuring approach with additional flexibility, accuracy, and a higher degree of process control. This has relevance for upgrading current laser processing technologies and offers a better understanding of the laser-induced physical processes, the nature of material modification, including the ability to identify competitive relaxation processes. The control factors were identified in the absorption phase, in the degree of non-equilibrium or nonlinearity of propagation, as well as in the succession of phase transitions. Consequently, using temporal pulse forming, control may be achieved on the chemical composition and the kinetic properties of the ablation products, as well as on the structural changes of the irradiated material and energy confinement on smallest spatial scales. The potential spectrum of applications ranges from quality structuring for increased functionality to integration in analytical methods sensitive to particle emission, however, designing material removal characteristics can be appealing for a broader range of applications. The results have documented the possibility to attain desired structural modifications in bulk transparent materials. Using these tools, it was e.g. possible to achieve refractive index changes in glasses which are otherwise difficult to process. Novel properties and functions are attached in this way to the material, laying a groundwork for adaptive optimization in material processing.

References

1. J.C. Diels, W. Rudolph, *Ultrashort Laser Pulse Phenomenon: Fundamentals,Techniques, and Applications on a Femtosecond Time Scale* (2nd edn., Academic Press, London, 2006)
2. C.E. Rulliere, *Femtosecond Laser Pulses. Principles and Experiments* (Springer, Berlin, 2004)

3. M. Wollenhaupt, A. Assion, T. Baumert, in *Springer Handbook of Lasers and Optics*, ed. by F. Träger (Springer Science + Business Media, New York, 2007)
4. I.V. Hertel, C.P. Schulz, *Atome, Moleküle und Optische Physik*, vol. 1 (Springer Verlag, Berlin Heidelberg, 2008)
5. A.M. Weiner, Prog. Quantum Electron. **19**, 161 (1995)
6. A. Präkelt, M. Wollenhaupt, C. Sarpe-Tudoran, T. Baumert, Phys. Rev. A **70**, 063407 (2004)
7. M. Wollenhaupt, A. Präkelt, C. Sarpe-Tudoran, D. Liese, T. Baumert, Appl. Phys. B: Laser Opt. **82**, 183 (2006)
8. J.D. McMullen, J. Opt. Soc. Am. B **67**, 1575 (1977)
9. R. Stoian, M. Boyle, A. Thoss, A. Rosenfeld, G. Korn, I.V. Hertel, Appl. Phys. A: Mat. Sci. Process. **77**, 265 (2003)
10. M. Renard, R. Chaux, B. Lavorel, O. Faucher, Opt. Exp. **12**, 473 (2004)
11. A.M. Weiner, D.E. Leaird, G.P. Wiederrecht, K.A. Nelson, Science **247**, 1317 (1990)
12. D. Meshulach, Y. Silberberg, Nature **396**, 239 (1998)
13. R.M. Koehl, K.A. Nelson, Chem. Phys. **267**, 151 (2001)
14. J.L. Herek, W. Wohlleben, R. Cogdell, D. Zeidler, M. Motzkus, Nature **417**, 533 (2002)
15. M. Wollenhaupt, A. Präkelt, C. Sarpe-Tudoran, D. Liese, T. Bayer, T. Baumert, Phys. Rev. A **73**, 063409 (2006)
16. D. Meshulach, Y. Silberberg, Phys. Rev. A **60**, 1287 (1999)
17. P. Panek, A. Becker, Phys. Rev. A **74**, 023408 (2006)
18. A.M. Weiner, Rev. Sci. Instrum. **71**, 1929 (2000)
19. M.M. Wefers, K.A. Nelson, J. Opt. Soc. Am. B **12**, 1343 (1995)
20. T. Tanabe, F. Kannari, F. Korte, J. Koch, B. Chichkov, Appl. Opt. **44**, 1092 (2005)
21. G. Vogt, P. Nuernberger, R. Selle, F. Dimler, T. Brixner, G. Gerber, Phys. Rev. A **74**, 033413 (2006)
22. T. Bayer, M. Wollenhaupt, T. Baumert, J. Phys. B: At. Mol. Phys. **41**, 074007 (2008)
23. A. Galler, T. Feurer, Appl. Phys. B: Laser Opt. **90**, 427 (2008)
24. B. von Vacano, T. Buckup, M. Motzkus, J. Opt. Soc. Am. B **24**, 1091 (2007)
25. M. Hacker, G. Stobrawa, T. Feurer, Opt. Exp. **9**, 191 (2001)
26. A. Rundquist, A. Efimov, D.H. Reitze, J. Opt. Soc. Am. B **19**, 2468 (2002)
27. T. Brixner, G. Gerber, Opt. Lett. **26**, 557 (2001)
28. T. Brixner, G. Krampert, T. Pfeifer, R. Selle, G. Gerber, M. Wollenhaupt, O. Graefe, C. Horn, T. Baumert, Phys. Rev. Lett **92**, 208301 (2004)
29. A.M. Weiner, J.P. Heritage, E.M. Kirschner, J. Opt. Soc. Am. B **5**, 1563 (1988)
30. M.M. Wefers, K.A. Nelson, Opt. Lett. **93**, 2032 (1993)
31. E. Zeek, K. Maginnis, S. Backus, U. Russek, M.M. Murnane, G. Mourou, H.C. Kapteyn, Opt. Lett. **24**, 493 (1999)
32. M. Hacker, G. Stobrawa, R.A. Sauerbrey, T. Buckup, M. Motzkus, M. Wildenhain, A. Gehner, Appl. Phys. B: Laser Opt. **76**, 711 (2003)
33. S.H. Shim, D.B. Strasfeld, E.C. Fulmer, M.T. Zanni, Opt. Lett. **31**, 838 (2006)
34. J.X. Tull, M.A. Dugan, W.S. Warren, in *Advances in Magnetic and Optical Resonance*, ed. by W.S. Warren (Academic Press, 1997)
35. D. Goswami, Phys. Rep. **374**, 385 (2003)
36. P. Tournois, Opt. Commun. **140**, 245 (1997)

37. F. Verluise, V. Laude, Z. Cheng, C. Spielmann, P. Tournois, Opt. Lett. **25**, 575 (2000)
38. J.C. Vaughan, T. Feurer, K.A. Nelson, J. Opt. Soc. Am. B **19**, 2489 (2002)
39. R.S. Judson, H. Rabitz, Phys. Rev. Lett. **68**, 1500 (1992)
40. T. Baumert, T. Brixner, V. Seyfried, M. Strehle, G. Gerber, Appl. Phys. B: Laser Opt. **65**, 779 (1997)
41. C.J. Bardeen, V.V. Yakolev, K.R. Wilson, S.D. Carpenter, P.M. Weber, W.S. Warren, Chem. Phys. Lett. **280**, 151 (1997)
42. D. Yelin, D. Meshulach, Y. Silberberg, Opt. Lett. **22**, 1793 (1997)
43. T. Back, *Evolutionary Algorithms in Theory and Practice* (University Press, New York, USA, 1996)
44. C. Siedschlag, O.M. Shir, T. Back, M.J.J. Vrakking, Opt. Commun. **264**, 511 (2006)
45. J.W. Wilson, P. Schlup, M. Lunacek, D. Whitley, R.A. Bartels, Rev. Sci. Instrum. **79**, 033103 (2008)
46. F. Dausinger, F. Lichtner, H. Lubatschowski, eds., *Femtosecond Technology for Technical and Medical Application* (Springer, Berlin Heidelberg, 2004)
47. H. Misawa, S. Juodkazis, eds., *3D Laser Microfabrication: Principles And Applications* (Wiley-VCH, Weinheim, 2006)
48. L.V. Keldysh, Sov. Phys. JETP **20**, 1307 (1965)
49. B.C. Stuart, M.D. Feit, A.M. Rubenchik, B.W. Shore, M.D. Perry, Phys. Rev. Lett. **74**, 2248 (1995)
50. A. Kaiser, B. Rethfeld, M. Vicanek, G. Simon, Phys. Rev. B **61**, 11437 (2000)
51. V.E. Gruzdev, Phys. Rev. B **75**, 205106 (2007)
52. A.C. Tien, S. Backus, H.C. Kapteyn, M.M. Murnane, G. Mourou, Phys. Rev. Lett. **82**, 3883 (1999)
53. M. Lenzner, J. Krüger, S. Sartania, Z. Cheng, C. Spielmann, G. Mourou, W. Kautek, F. Krausz, Phys. Rev. Lett. **80**, 4076 (1989)
54. S.S. Mao, F. Qu'er'e, S. Guizard, X. Mao, R.E. Russo, G. Petite, P. Martin, Appl. Phys. A: Mat. Sci. Process. **79**, 1695 (2004)
55. V.V. Temnov, K. Sokolowski-Tinten, P. Zhou, A. El-Khamhawy, D. von der Linde, Phys. Rev. Lett. **97**, 237403 (2006)
56. I.H. Chowdhury, X. Xu, A.M. Weiner, Appl. Phys. Lett. **86**, 151110 (2005)
57. C. Sarpe-Tudoran, A. Assion, M. Wollenhaupt, M. Winter, T. Baumert, Appl. Phys. Lett. **88**, 261109 (2006)
58. B. Rethfeld, Phys. Rev. Lett. **92**, 187401 (2004)
59. E. Louzon, Z. Henis, S. Pecker, Y. Ehrlich, D. Fisher, M. Fraenkel, A. Zigler, Appl. Phys. Lett. **87**, 241903 (2005)
60. R. Stoian, M. Boyle, A. Thoss, A. Rosenfeld, G. Korn, I.V. Hertel, E.E.B. Campbell, Appl. Phys. Lett. **80**, 353 (2002)
61. P.R. Herman, R.S. Marjoribanks, Appl. Surf. Science **154**, 577 (2000)
62. I.M. Burakov, N.M. Bulgakova, R. Stoian, A. Rosenfeld, I.V. Hertel, Appl. Phys. A: Mat. Sci. Process. **81**, 1639 (2005)
63. L. Englert, B. Rethfeld, L. Haag, M. Wollenhaupt, C. Sarpe-Tudoran, T. Baumert, Opt. Exp. **15**, 17855 (2007)
64. L. Englert, M. Wollenhaupt, L. Haag, C. Sarpe-Tudoran, B. Rethfeld, T. Baumert, Appl. Phys. A: Mat. Sci. Process. **92**, 749 (2008)
65. M. Merano, G. Boyer, A. Trisorio, G. Chriaux, G. Mourou, Opt. Lett. **32**, 2239 (2007)

66. K. Eidmann, J. Meyer-ter Vehn, T. Schlegel, H. S., Phys. Rev. E **62**, 1202 (2000)
67. J. Solis, C.N. Afonso, J.F. Trull, M.C. Morilla, Appl. Phys. **75**, 7788 (2008)
68. M. Spyridaki, E. Koudoumas, P. Tzanetakis, C. Fotakis, R. Stoian, A. Rosenfeld, I.V. Hertel, Appl. Phys. Lett. **83**, 1474 (2003)
69. I.H. Chowdhury, X. Xu, A.M. Weiner, in *Commercial and biomedical applications of ultrafast lasers III*, *Proceedings of SPIE*, vol. 4978, ed. by Neev, J. and Ostendorf, A. and Schaffer, C. B. (SPIE, Bellingham, 2003), p. 138
70. Y. Prior, K.Y. Zhang, V. Batenkov, Y. Paskover, J.H. Klein-Wiele, P. Simon, in *High-Power Laser Ablation V*, *Proceedings of SPIE*, vol. 5448, ed. by Phipps, C.R. (SPIE, Bellingham, 2004), p. 1049
71. R. Hergenröder, M. Miclea, V. Hommes, Nanotechnology **17**, 4065 (2006)
72. H. Dachraoui, W. Husinsky, Phys. Rev. Lett. **97**, 107601 (2006)
73. R. Stoian, A. Mermillod-Blondin, A. Rosenfeld, I.V. Hertel, M. Spyridaki, E. Koudoumas, P. Tzanetakis, C. Fotakis, N.M. Bulgakova, Appl. Phys. Lett. **87**, 124105 (2005)
74. J.P. Colombier, P. Combis, A. Rosenfeld, I.V. Hertel, E. Audouard, R. Stoian, Phys. Rev. B **74**, 224106 (2006)
75. A.Q. Wu, X. Xu, Appl. Phys. Lett. **90**, 251111 (2007)
76. J.P. Colombier, E. Audouard, P. Combis, A. Rosenfeld, I.V. Hertel, R. Stoian, Appl. Surf. Sci. (submitted 2008)
77. A. Assion, M. Wollenhaupt, L. Haag, F. Maiorov, C. Sarpe-Tudoran, M. Winter, U. Kutschera, T. Baumert, Appl. Phys. B: Laser Opt. **77**, 391 (2003)
78. A. Klini, P. Loukakos, D. Gray, A. Manousaki, C. Fotakis, Opt. Exp. **16**, 11300 (2008)
79. K. Itoh, W. Watanabe, S. Nolte, C. Schaffer, MRS Bull. **31**, 620 (2006)
80. I.M. Burakov, N.M. Bulgakova, R. Stoian, A. Mermillod-Blondin, E. Audouard, A. Rosenfeld, A. Husakou, I.V. Hertel, J. Appl. Phys. **101**, 043506 (2007)
81. R.R. Gattass, E. Mazur, Nat. Photonics **2**, 219 (2008)
82. G. Cerullo, R. Osellame, S. Taccheo, M. Marangoni, D. Polli, R. Ramponi, P. Laporta, S. De Silvestri, Opt. Lett. **27**, 1938 (2002)
83. Y. Cheng, K. Sugioka, K. Midorikawa, M. Masuda, K. Toyoda, K. Kawachi, K. Shihoyama, Opt. Lett. **28**, 55 (2003)
84. S. Nolte, M. Will, J. Burghoff, A. Tünnermann, Appl. Phys. A: Mat. Sci. Process. **77**, 109 (2003)
85. R.R. Thomson, A.S. Bockelt, E. Ramsey, S. Beecher, A.H. Greenway, A.K. Kar, D.T. Reid, Opt. Express **16**, 12786 (2008)
86. A. Mermillod-Blondin, I.M. Burakov, Y.P. Meshcheryakov, N.M. Bulgakova, E. Audouard, A. Rosenfeld, A. Husakou, I.V. Hertel, Phys. Rev. B **77**, 104205 (2008)
87. W. Gawelda, D. Puerto, J. Siegel, A. Ferrer, A. Ruiz de la Cruz, H. Fernandez, J. Solis, Appl. Phys. Lett. **93**, 121109 (2008)
88. G. Heck, J. Sloss, R.J. Levis, Opt. Commun. **259**, 216 (2006)
89. R. Ackermann, E. Salmon, N. Lascoux, J. Kasparian, P. Rohwetter, K. Stelmaszczyk, S. Li, A. Lindinger, L. Wöste, P. Béjot, L. Bonacina, Appl. Phys. Lett. **89**, 171117 (2006)
90. M.Y. Shverdin, S.N. Goda, G.Y. Yin, S.E. Harris, Opt. Lett. **31**, 1331 (2006)
91. A. Mermillod-Blondin, C. Mauclair, A. Rosenfeld, J. Bonse, I.V. Hertel, E. Audouard, R. Stoian, Appl. Phys. Lett. **93**, 021921 (2008)
92. M. Ams, G.D. Marshall, D.J. Spence, M.J. Withford, Opt. Express **13**, 5676 (2005)

Index